Au$_{40}$(SR)$_{24}$ Cluster as a Chiral Dimer of 8-Electron Superatoms: Structure and Optical Properties

Sami Malola,[†] Lauri Lehtovaara,[†] Stefan Knoppe,[‡] Kuo-Juei Hu,[§] Richard E. Palmer,[§] Thomas Bürgi,[‡] and Hannu Häkkinen*[,†,⊥]

[†]Department of Chemistry, Nanoscience Center, University of Jyväskylä, FI-40014 Jyväskylä, Finland
[‡]Department of Physical Chemistry, University of Geneva, 1211 Geneva 4, Switzerland
[§]Nanoscale Physics Research Laboratory, School of Physics and Astronomy, University of Birmingham, Birmingham B15 2TT, U.K.
[⊥]Department of Physics, Nanoscience Center, University of Jyväskylä, FI-40014 Jyväskylä, Finland

S *Supporting Information*

ABSTRACT: We predict and analyze density-functional theory (DFT)-based structures for the recently isolated Au$_{40}$(SR)$_{24}$ cluster. Combining structural information extracted from ligand-exchange reactions, circular dichroism and transmission electron microscopy leads us to propose two families of low-energy structures that have a chiral Au−S framework on the surface. These families have a common geometrical motif where a nonchiral Au$_{26}$ bi-icosahedral cluster core is protected by 6 RS−Au−SR and 4 RS−Au−SR−Au−SR oligomeric units, analogously to the "Divide and Protect" motif of known clusters Au$_{25}$(SR)$_{18}$$^{−/0}$, Au$_{38}(SR)_{24}$ and Au$_{102}$(SR)$_{44}$. The strongly prolate shape of the proposed Au$_{26}$ core is supported by transmission electron microscopy. Density-of-state-analysis shows that the electronic structure of Au$_{40}$(SR)$_{24}$ can be interpreted in terms of a dimer of two 8-electron superatoms, where the 8 shell electrons are localized at the two icosahedral halves of the metal core. The calculated optical and chiroptical characteristics of the optimal chiral structure are in a fair agreement with the reported data for Au$_{40}$(SR)$_{24}$.

Use of atomically well-defined, ligand-stabilized 1−3 nm gold clusters is expected to open new avenues for studies in diverse fields such as molecular electronics, imaging of biomolecules and bionanoparticles, chiral recognition, and chiral catalysis. Air-stable, electrochemically stable, and thermally stable thiolate-stabilized gold clusters, Au$_x$(SR)$_y$, form a special subclass of these clusters. Their synthesis and experimental and theoretical characterization have advanced tremendously over the last several years.[1−9]

It is now widely accepted that, in general, the specific properties of molecularly well-defined Au$_x$(SR)$_y$ clusters with 1−2 nm metal cores arise from the detailed interplay between the quantum confinement of Au(6s) electrons in the core and the gold−thiolate surface chemistry. Quantum confinement effects are well-known from studies of metal clusters in gas phase,[10] and recently, large-scale electronic structure analysis has clearly demonstrated their crucial role also for the stabilization of the electronic structure of several structurally known thiolate monolayer-protected gold clusters.[3,9,11−13]

Electronic structure and optical properties are currently well understood for the few clusters where the crystal structure is available: Au$_{102}$(p-MBA)$_{44}$ (p-MBA = p-mercaptobenzoic acid),[14] anionic and neutral Au$_{25}$(2-PET)$_{18}$[15−17] and Au$_{38}$(2-PET)$_{24}$ (2-PET = 2-phenylethylthiolate SCH$_2$CH$_2$Ph).[18] The clusters have shell-closing electron numbers[11] such as 58 (Au$_{102}$, approximately spherical core), 8 (Au$_{25}$ anion, approximately spherical core), and 14 (Au$_{38}$, a prolate core).

The Au$_{40}$(2-PET)$_{24}$ cluster was isolated only recently, and its total structure determination is not available.[19] Using insight gained from existing experimental characterization of the Au$_{40}$(2-PET)$_{24}$ cluster via ligand-exchange reactions and chiroptical spectroscopy[20−22] and new information from transmission electron microscopy presented here, we hereby construct models for the structure of the Au$_{40}$(SR)$_{24}$ cluster and analyze them in detail via DFT computations. We propose a set of structures that reproduce essentially all the available information from experimental characterizations of this cluster. The electronic structure analysis further shows that the shell electron count of 16 for Au$_{40}$(SR)$_{24}$ can be understood from a concept where two 8-electron "superatoms" form an interacting dimer in the metal core, connected also by the chiral gold−thiolate overlayer. This is the first report on a dimeric electronic (and geometric) composition of an all-thiolate-protected gold nanocluster and thus advances our fundamental understanding of the interplay of electronic structure and atomic geometry of 1−3 nm Au$_x$(SR)$_y$ clusters.

All the DFT computations utilized the GPAW program package.[23] Total energies and optical properties were evaluated at the GGA-PBE level (gradient-corrected functional of Perdew, Burke, and Ernzerhof).[24] The computational method is the same as the previous one used by us successfully for several other thiolate-stabilized gold clusters[11−13] (details are given in the Supporting Information (SI) text).

We found two closely related families (hereafter denoted as **A** and **B**) of potential structures that agree with most of the previously reported experimental observations on Au$_{40}$(2-PET)$_{24}$. Both structure families have a common Au$_{26}$ core: a dimer of two Au$_{13}$ icosahedrons having an edge−edge contact, rotated by 90° with respect to each other (Figure 1). The core
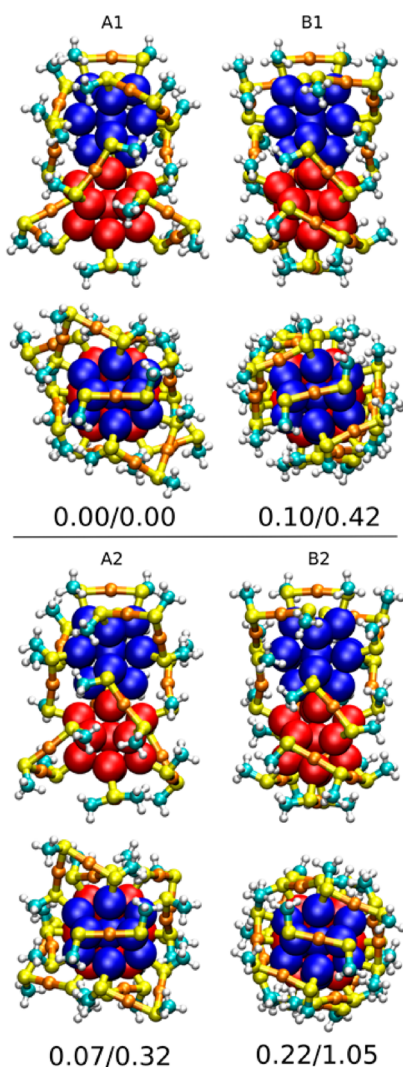
Figure 1. Side- and top-view illustrations of structures **A1**, **A2**, **B1**, and **B2** (with methylthiolates as SR). Blue and red spheres denote the two Au$_{13}$ icosahedra making the dimeric metal core, giving an aspect ratio of ∼2. The icosahedra make edge-to-edge contacts with 90° rotation. Au(I) atoms in the gold−thiolate units are denoted by the small orange spheres, and sulfur atoms, by the yellow spheres. The long gold−thiolate units adopt a screw-like arrangement along the C$_2$ axis (C$_2$ axis visible in the top views). For structures A1 and B1 the handedness of the screw formed by the long units is identical for both hemispheres, thus forming a chiral Au−S framework, whereas for structures **A2** and **B2** the handedness is opposite in the two hemispheres. The two numbers for each structure are relative GGA-PBE total energies (in eV) calculated for optimized structures with SH and SCH$_3$ ligands, respectively.

is nonchiral, and in an idealized symmetry it has three C$_2$ rotation axes, 2 σ$_v$ reflection planes, and one S$_4$ improper rotation axis. The icosahedral subunits are connected in the "waist" region by four short RS−Au−SR units and the "pole" regions are both capped by one short unit and two long RS−Au−SR−Au−SR units. In the "Divide and Protect" scheme,[25] the composition of the cluster can thus be written as Au$_{40}$(SR)$_{24}$ = Au$_{26}$(RS−Au−SR)$_6$(RS−Au−SR−Au−SR)$_4$. The difference between families **A** and **B** arises from the way in which the long gold−thiolate units are bound to the core. In family **A**, the units are bound to gold core atoms that are nearest neighbors, whereas in family **B** the units cap next-

nearest-neighbor core atoms. In both families, we have identified one structure with three C$_2$ rotational axes for the Au−S framework in the protecting layer. We denote these structures as **A1** and **B1**. Note that the Au−S framework of these structures is chiral. There is a large number of additional Au−S framework structures that have an additional S$_4$ improper rotation axis in the Au−S overlayer. The framework of these structures is therefore achiral. However, these clusters become chiral through the orientation of the −SR groups. We denote the energy-optimal structures of these subclasses as **A2** and **B2**. The four structures **A1**, **A2**, **B1**, and **B2** optimized with the methylthiolate ligand are shown in Figure 1. We note that for each of these, there is a large number for conformers (structures where the −SR groups vary with respect to cis−trans configurations within the gold−thiolate units).

Structures **A1**, **A2**, **B1**, and **B2** are related to the predicted[13] and observed[18] structures of the slightly smaller Au$_{38}$(SR)$_{24}$ that has a composition of Au$_{23}$(RS−Au−SR)$_3$(RS−Au−SR−Au−SR)$_6$ with a face-fused bi-icosahedral Au$_{23}$ core and a chiral D$_3$ Au−S framework configuration of the protecting gold−thiolate units. That core is strongly prolate, as was observed also from HAADF-STEM studies of Au$_{38}$(SR)$_{24}$ clusters on a solid support, giving an aspect ratio of about 1.5.[26]
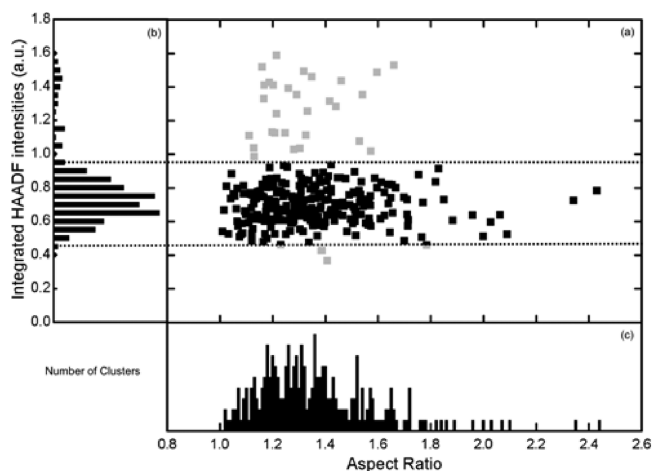

Figure 2. Analysis of the aspect ratios for Au$_{40}$(2-PET)$_{24}$ cluster sample as measured via HAADF-STEM. (a) Statistical distribution of HAADF intensities as a function of measured aspect ratio. (b) Corresponding histogram. (c) Histogram of aspect ratios of cluster monomers, obtained by excluding all particles outside the HAADF intensities range marked by the dotted lines in (a).

A similar HAADF-STEM analysis was done now for a sample of Au$_{40}$(2-PET)$_{24}$ clusters, and the result is shown in Figure 2 (further details of the analysis are discussed in the SI). Compared to the known Au$_{38}$ case,[18,26] the current analysis suggests that the core aspect ratio has a maximal value in the range of 1.8−2.1, i.e, clearly higher than in the case of Au$_{38}$. This result fits in with all the predicted structures shown in Figure 1.

Relative total energies (GGA-PBE) and HOMO−LUMO energy gaps E$_g^{HL}$ of **A1**, **A2**, **B1**, and **B2** are shown in Figure 1 and Table S1 (SI). The shell-electron counts[11] of Au$_{38}$(SR)$_{24}$ and Au$_{40}$(SR)$_{24}$ are 14 and 16, respectively. Jellium models for electron-gas clusters[27] predict that at these electron numbers the cluster should have a strong spheroidal deformation (prolate or oblate). DFT molecular dynamics simulations

have also shown that monovalent metal (such as sodium) clusters of 14 and 16 valence electrons adopt strongly deformed shapes.[28] In this work we searched also for alternative shapes (oblate and tetrahedral) for the core of $Au_{40}(SR)_{24}$, but all the attempts led to structures that have very unfavorable energies compared to those of **A1**, **A2**, **B1**, and **B2**.

The count of 16 shell-electrons in $Au_{40}(SR)_{24}$ can be explained by analyzing the electronic states through a local projection of orbitals into each of the Au_{13} icosahedral units of the core. Figure S1 (SI) shows the projection for structure **A1**; the other low-energy structures shown in Figure 1 give a similar result. Around the HOMO−LUMO gap, one sees a clear change in the angular momentum characteristics of the Au(6s)-derived states from a global *P*-like symmetry to *D*-like symmetry ($L = 1 \rightarrow 2$). Closing of the P-shell indicates 8 s-like "free" electrons in each Au_{13} unit, giving a total of 16 s-electrons for the metal core. Overall, each half of the full cluster can be regarded as a $Au_{13}(AuSR)_3(Au_2(SR)_3)_2$ subsystem. Since each gold−thiolate unit localizes one Au(6s) electron from the core, one arrives at the count of $13 - 5 = 8$ for each subsystem.
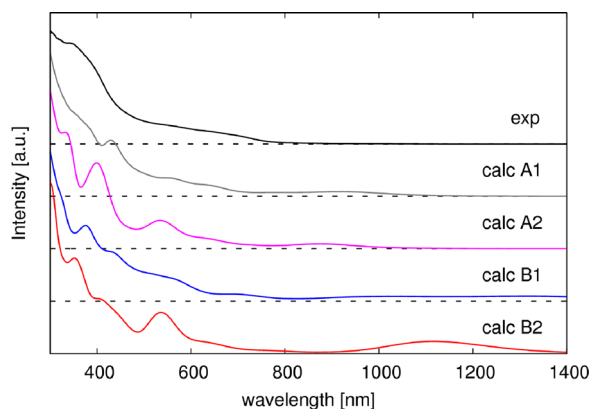

Figure 3. The experimental (black curve) optical absorption spectrum of $Au_{40}(2\text{-PET})_{24}$ (ref 22) and the calculated LR-TDDFT spectra for structures **A1**, **A2**, **B1**, and **B2**. In the LR-TDDFT spectra, the single oscillator strengths are folded by 0.1 eV Gaussians. SH groups are used to model SR in the calculation.

Figure 3 shows a comparison of the calculated LR-TDDFT spectra of **A1**, **A2**, **B1**, and **B2** to the previously measured[22] optical absorption spectrum of $Au_{40}(2\text{-PET})_{24}$. The experimental spectrum displays an onset of electronic transitions in the range 750−800 nm. It is seen that the overall chiral **A1** and **B1** structures yield the best agreement to the experiment, particularly the shape of the LR-TDDFT spectrum of **A1** is very close to the experimental one, also by comparison of derivative spectra as displayed in Figure S2 (SI). A very broad weak feature in the range of 700−1000 nm in the LR-TDDFT spectrum of **A1** is due to several optically forbidden low-lying transitions of mainly $\pi-\pi$ metal-to-metal character that dominate the energy region close to the HOMO−LUMO gap. The π-character of the states in the core arises from coupling of the *P* and *D* symmetric states of each 8-electron subsystem (not shown here).

The measured[22] circular dichroism (CD) spectrum of $Au_{40}(2\text{-PET})_{24}$ contains rich additional information about the electronic states and provides a stringent test for theory. Here, we recalculated the published[13] theoretical CD spectrum of the structurally known chiral $Au_{38}(SR)_{24}$ cluster. This cluster

provides an ideal test case since very recently, CD spectra was measured from enantiopure samples of $Au_{38}(2\text{-PET})_{24}$.[29] Comparison of our calculated (at the GGA-PBE level) and experimental CD spectra of $Au_{38}(2\text{-PET})_{24}$ in Figure S3 (SI) shows that our calculation is able to reproduce eight measured CD signals (polarities down to around 400 nm).
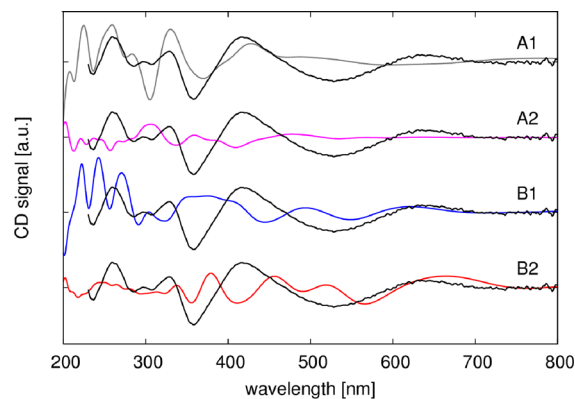

Figure 4. Calculated CD spectra of structures **A1**, **A2**, **B1**, and **B2** as compared to the experimental CD spectrum (black curve) of $Au_{40}(2\text{-PET})_{24}$ (ref 22). The transitions are folded by 0.1 eV Gaussians. SH groups are used to model SR in the calculation.

Figure 4 shows a comparison of the calculated CD spectra of **A1**, **A2**, **B1**, and **B2** to the published CD spectrum of $Au_{40}(2\text{-PET})_{24}$. Overall, the chiral structures **A1** and **B1** produce CD signals that are stronger than the ones from **A2** and **B2**. We observe that while the higher-energy **B1** isomer reproduces better the lowest-energy transitions in the range 550−700 nm, the optimal-energy **A1** structure yields the best agreement in the higher-energy range of transitions below 450 nm. In fact, a pattern of four experimental CD signals is reproduced by **A1** in the range of 250−450 nm.

The bonding environment of the sulfur atom connecting a gold−thiolate unit to the gold core has four nonequivalent directions: Au(0) in the core, R, Au(I) in the unit, and the lone pair. This fact renders each sulfur atom as a stereogenic center. This explains why structures with a nonchiral Au−S framework (e.g., **A2** and **B2**) give CD signals in our calculations. We expect that **A1** should dominate the experimental spectrum, however coexistence and contribution from isomers cannot be ruled out at the moment.[22] The fact that the calculated CD spectrum of **A1** is not in a "perfect" agreement (at the level of the benchmarked $Au_{38}(SR)_{24}$) with the experimental data may be due to effects from *cis-trans* conformations in the ligand layer, whose realistic energetics may need further calculations with the full 2-PET ligand to account for the steric effects and to find the correct (if there is only one) *cis−trans* conformer.

The composition $Au_{40}(SR)_{24}$ = $Au_{26}(RS−Au−SR)_6(RS−Au−SR−Au−SR)_4$ of **A1**, **A2**, **B1**, and **B2** gives an interesting implication for ligand-exchange. Among the six short gold−thiolate units, four are equivalent and should have an exchange rate that is different from the other two units on the poles of the cluster. It is notable that both this composition and two different exchange rates for the shorter units have already been postulated from the analysis of ligand-exchange reactions of $Au_{40}(2\text{-PET})_{24}$ with bidentate 1,1′-binapththyl-2,2′-dithiol (ref 20).

In summary, our DFT calculations predict a novel geo-metrical motif for the experimentally, yet unresolved,

$Au_{40}(SR)_{24}$ cluster. The core of this cluster is a dimer of two icosahedral Au_{13} units that each localize 8 Au(6s) free electrons to yield the total of 16 shell electrons. Two low-energy "full-chiral" geometries **A1** and **B1** were found, from which **A1** has the lower energy and gives a better match with the measured linear absorption and CD spectra. In addition, a number of low-energy structures (and conformers) are predicted which have local chirality in the ligand layer. These isomers might be populated in the synthesis.[22]

Finally, our results open a new alternative avenue to explain compositions of a few yet unknown $Au_x(SR)_y$ clusters. It is conceivable that the metal cores of some of the larger clusters in fact are composed of trimeric, tetrameric, etc. configurations of the icosahedral Au_{13} units. For example, one can build a linear trimeric cluster $Au_{57}(SR)_{32}$ with 25 shell electrons with the "Divide and Protect" composition of $Au_{39}(RS-Au-SR)_{10}(RS-Au-SR-Au-SR)_4$ that is a direct extension of structures shown in Figure 1. In a cationic form, such a cluster would also be electronically a trimer of 8-electron superatoms $(3 \times 8 = 24)$. It is notable that alkanethiolate-stabilized gold clusters of that size range have been reported, such as $Au_{54}(SR)_{30}$ and $Au_{55}(SR)_{31}$.[30]

■ ASSOCIATED CONTENT

Ⓢ Supporting Information

GPAW computational details, analysis of the electronic structure of **A1**, derivative of optical spectra of **A1** and experiment, CD spectrum of the known $Au_{38}(SR)_{24}$, experimental details on the $Au_{40}(2\text{-PET})_{24}$ synthesis and HAADF-STEM analysis, additional $Au_{40}(SR)_{24}$ structures and coordinates of **A1** and **B1**, full ref 23. This material is available free of charge via the Internet at http://pubs.acs.org.

■ AUTHOR INFORMATION

Corresponding Author
hannu.j.hakkinen@jyu.fi

Notes
The authors declare no competing financial interest.

■ ACKNOWLEDGMENTS

■ REFERENCES

(1) Templeton, A. C.; Wuelfing, W. P.; Murray, R. W. *Acc. Chem. Res.* **2000**, *33*, 27.
(2) Daniel, M.-C.; Astruc, D. *Chem. Rev.* **2004**, *104*, 293.
(3) Häkkinen, H. *Chem. Soc. Rev.* **2008**, *37*, 1847.
(4) Sardar, R.; Funston, A. M.; Mulvaney, O.; Murray, R. W. *Langmuir* **2009**, *25*, 13840.
(5) Jin, R. C. *Nanoscale* **2010**, *2*, 343.
(6) Tsukuda, T. *Bull. Chem. Soc. Jpn.* **2012**, *85*, 151.
(7) Häkkinen, H. *Nature Chem.* **2012**, *4*, 443.
(8) Gautier, C.; Bürgi, T. *ChemPhysChem* **2009**, *10*, 483.
(9) Aikens, C. M. *J. Phys. Chem. Lett.* **2011**, *2*, 99.
(10) deHeer, W. A. *Rev. Mod. Phys.* **1993**, *65*, 611.
(11) Walter, M.; Akola, J.; Lopez-Acevedo, O.; Jadzinsky, P. D.; Calero, G.; Ackerson, C. J.; Whetten, R. L.; Gronbeck, H.; Hakkinen, H. *Proc. Natl. Acad. Sci. U.S.A.* **2008**, *105*, 9157.
(12) Akola, J.; Walter, M.; Whetten, R. L.; Häkkinen, H.; Grönbeck, H. *J. Am. Chem. Soc.* **2008**, *130*, 3756.
(13) Lopez-Acevedo, O.; Tsunoyama, H.; Tsukuda, T.; Hakkinen, H.; Aikens, C. M. *J. Am. Chem. Soc.* **2010**, *132*, 8210.
(14) Jadzinsky, P. D.; Calero, G.; Ackerson, C. J.; Bushnell, D. A.; Kornberg, R. D. *Science* **2007**, *318*, 430.
(15) Heaven, M. W.; Dass, A.; White, P. S.; Holt, K. M.; Murray, R. W. *J. Am. Chem. Soc.* **2008**, *130*, 3754.
(16) Zhu, M.; Aikens, C. M.; Hollander, F. J.; Schatz, G. C.; Jin, R. C. *J. Am. Chem. Soc.* **2008**, *130*, 5883.
(17) Zhu, M.; Eckenhoff, W. T.; Pintauer, T.; Jin, R. *J. Phys. Chem. C* **2008**, *112*, 14221.
(18) Qian, H.; Eckenhoff, W. T.; Zhu, Y.; Pintauer, T.; Jin, R. *J. Am. Chem. Soc.* **2010**, *132*, 8280.
(19) Qian, H.; Zhu, Y.; Jin, R. *J. Am. Chem. Soc.* **2010**, *132*, 4583.
(20) Knoppe, S.; Dharmaratne, A. C.; Schreiner, E.; Dass, A.; Burgi, T. *J. Am. Chem. Soc.* **2010**, *132*, 16783.
(21) Knoppe, S.; Dass, A.; Burgi, T. *Nanoscale* **2012**, *4*, 4211.
(22) Knoppe, S.; Dolamic, I.; Dass, A.; Burgi, T. *Angew. Chem., Int. Ed.* **2012**, *51*, 7589. In this work, the HPL chromatogram of $Au_{40}(2\text{-PET})_{24}$ shows several minor peaks besides that of the dominant species, which might be due to coexisting isomers.
(23) Enkovaara, J.; et al. *J. Phys.: Condens. Matter* **2010**, *22*, 253202.
(24) Perdew, J. P.; Burke, K.; Ernzerhof, M. *Phys. Rev. Lett.* **1996**, *77*, 3865.
(25) Häkkinen, H.; Walter, M.; Grönbeck, H. *J. Phys. Chem. B* **2006**, *110*, 9927.
(26) Wang, Z. W.; Toikkanen, O.; Quinn, B. M.; Palmer, R. E. *Small* **2011**, *7*, 1542.
(27) Koskinen, M.; Lipas, P. O.; Manninen, M. *Z. Phys. D* **1995**, *35*, 285.
(28) Häkkinen, H.; Manninen, M. *Phys. Rev. B* **1995**, *52*, 1540. Moseler, M.; Huber, B.; Häkkinen, H.; Landman, U.; Wrigge, G.; Hoffman, M. A.; von Issendorff, B. *Phys. Rev. B* **2003**, *68*, 165413.
(29) Dolamic, I.; Knoppe, S.; Dass, A.; Burgi, T. *Nat. Commun.* **2012**, *3*, 798.
(30) Tsunoyama, R.; Tsunoyama, H.; Pannopard, P.; Limtrakul, J.; Tsukuda, T. *J. Phys. Chem. C* **2010**, *114*, 16004.